CORE
Metadata, citation and similar papers at core.ac.uk
Provided by Explore Bristol Research

Cicek, K., & Cryan, M. (2018). Spectral analysis of a four-port DBR micro-ring resonator for spectral sensing applications. *Journal of Optics*, *20*(8), [085803]. https://doi.org/10.1088/2040-8986/aad267

Peer reviewed version

License (if available):
Other

Link to published version (if available):
10.1088/2040-8986/aad267

Link to publication record in Explore Bristol Research
PDF-document

This is the accepted author manuscript (AAM). The final published version (version of record) is available online via IOP at https://doi.org/10.1088/2040-8986/aad267 . Please refer to any applicable terms of use of the publisher.

University of Bristol - Explore Bristol Research

General rights

This document is made available in accordance with publisher policies. Please cite only the published version using the reference above. Full terms of use are available:
http://www.bristol.ac.uk/pure/about/ebr-terms

Spectral Analysis of a Four-Port DBR Micro-Ring Resonator for Spectral Sensing Applications

K. Cicek

Department of Electrical and Electronics Engineering, Iğdır University, Iğdır, Turkey
Department of Electrical and Electronics Engineering, Merchant Venturers School of Engineering, University of Bristol, Bristol UK

E-mail: eexkc@my.bristol.ac.uk

Martin Cryan

Department of Electrical and Electronics Engineering, Merchant Venturers School of Engineering, University of Bristol, Bristol UK

March 2018

Abstract. In this paper, the spectral analysis of a fourport distributed Bragg reflector-micro ring resonator (DBR–MRR) is studied both analytically and numerically. First, the basic theory of the DBR–MRR is discussed and the effect of DBRs on resonant mode-split is studied analytically. Then the theory is supported with a numerical study using the Finite Difference Time Domain method. Finally, a potential application of the proposed structure is discussed: a sensor that keeps the concentration of a substance within a desired range, a concentration range controller.

1. Introduction

Micro Ring Resonators (MRR) are essential elements for a variety of photonic and optoelectronic applications, serving as vortex beam emitters or receivers [1], wavelength filters [2], laser cavities [3], optical switches [4] and optical sensors [5].The basic configuration of an MRR consists of a cavity-ring waveguide evanescently coupled to one or two access waveguides. MRRs possess unidirectional mode spectrum in a typical case unless any non-ideality introduced to the cavity; presence of an intracavity scattering element or surface roughness etc [6]. In case of a non-ideality, the counter-propagating modes are generated in the ring cavity which could result in resonance-split caused by lifting the degeneracy with intercoupling in between [7, 8]. Many theoretical and practical designs have been proposed to optimize and exploit this resonance response of MRRs using various methods. Latterly, the operational principle of split modes in MRRs has been proposed for spectral sensing applications which has attracted a significant level of interest due to the MRRs high level of sensitivity [9, 6, 10]. Several configurations of MRR spectroscopic sensors utilising the split mode feature arising

from the presence of an intracavity scattering element or surface roughness are studied that aim to provide a new generation of optical technologies which perform better in terms of optical sensing [7, 8, 11]. The mode-splitting technique has enabled the possibility of high sensitivity particle detection [11, 12], strain measurement [13], optical bend sensing [14], defect sensing in carbon nanotubes [15] etc... Recently, it has been demonstrated that MRR systems that includes distributed Bragg reflectors (DBRs) also exhibit split modes in their spectral response also making them a candidate for spectral sensors [16, 17]. In this study, we realised that counter–propagating modes of MRR that introduced by this DBRs, exhibit different degree of resonant–splitting which is the first demonstration in the literature, according to our knowledge. We have applied this to an optical sensing concept, a concentration range sensor, to provide a practical and easy monitoring of a particular substance within a mixture. Generally, the MRR-based optical concentration sensors are based on spectral resonance shift in response to concentration change [18, 5, 19]. In order to observe the concentration of a substance to be within a range with such sensors, the spectral shift corresponds to unit concentration needs to be calculated then required amount of shift for upper and lower level taken into consideration during the analysis. However, with the sensing concept we introduced here, the target concentration range can be observed directly from the spectrum analyser simply by following the splitting behaviour of the counter-propagating modes.

Here, the potential of proposed technique for optical concentration sensing is investigated. In accordance with this purpose, semi-analytical and finite difference time domain (FDTD) models are developed and results are presented. The outcome of the study indicates that the resonant modesplitting operation in the DBR–MRR geometry can be applied to sense the concentration of a certain substance within a desired range.

2. Analysis

2.1. Analytical Model

A basic configuration of a DBR–MRR geometry is sketched in Fig. 1(a). The system consists of an MRR coupled to two access waveguides and a DBR grating set placed on top of the MRR. As shown in the figure, whispering gallery modes (WGMs) of the MRR which are excited through the input port (E_i) propagate in clock-wise (CW) direction within the resonator and couple out from the Drop 1 port (D_1). Due to existence of the DBR scattering elements in the system, partially reflected WGMs build up counter–propagated modes in the counter clock–wise direction (CCW) and couple out from the Drop 2 port (D_2). With the assumption of lossless coupling, the interaction of the aforementioned modes and others displayed in Fig. 1(a) can be modelled by the matrix relations as shown in equations (1)-(6) [20, 21].

$$\begin{pmatrix} CW_1 \\ E_T \end{pmatrix} = K \begin{pmatrix} CW_4 \\ E_i \end{pmatrix} \tag{1}$$

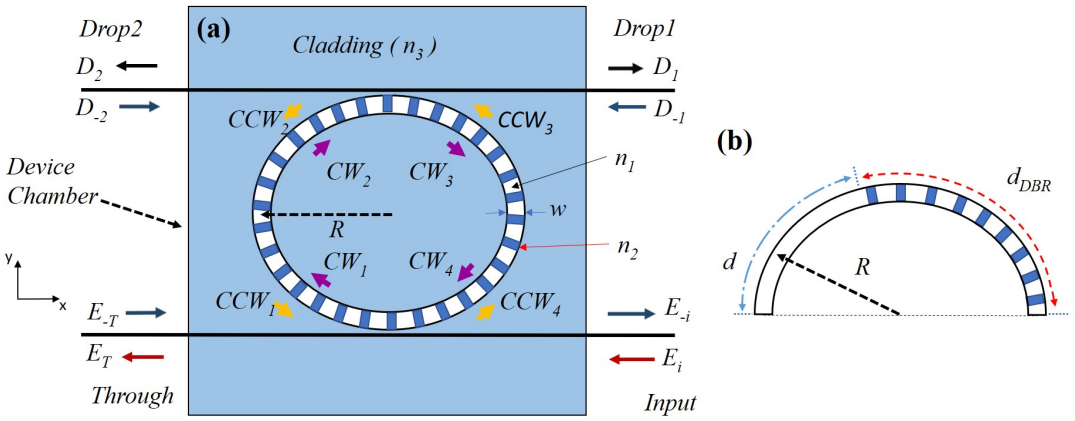

Figure 1: (a) Schematic architecture of proposed device which consists of a four–port MRR and a set of DBR gratings on top where Duty–cycle (D_{cy}) is the unetched portion of a full DBR period (P) which is expressed as a percentage in this study, n_2 and n_1 are the effective refractive indices of the unetched and etched portions of the grating, respectively and n_3 is the refractive index of the sensing medium. (b) Schematic diagram of a DBR–MRR. d_{DBR} is the length of DBRs and, d is the lengths of the MRR excluding the DBRs.

$$\begin{pmatrix} CW_2 \\ CCW_1 \end{pmatrix} = \alpha S e^{j\theta} \begin{pmatrix} CCW_2 \\ CW_1 \end{pmatrix} \tag{2}$$

$$\begin{pmatrix} CW_4 \\ CCW_3 \end{pmatrix} = \alpha S e^{j\theta} \begin{pmatrix} CCW_4 \\ CW_3 \end{pmatrix} \tag{3}$$

$$\begin{pmatrix} CW_3 \\ D_1 \end{pmatrix} = K \begin{pmatrix} CW_2 \\ D_{-2} \end{pmatrix} \tag{4}$$

$$\begin{pmatrix} CCW_2 \\ D_2 \end{pmatrix} = K \begin{pmatrix} CCW_3 \\ D_{-1} \end{pmatrix} \tag{5}$$

$$\begin{pmatrix} CCW_4 \\ E_{-i} \end{pmatrix} = K \begin{pmatrix} CCW_1 \\ E_{-T} \end{pmatrix} \tag{6}$$

Here CW_*, CCW_*, E_*, D_* represent the amplitudes of the electric fields in the presented directions and the points in the sketch. All the losses occurring along the propagation of the beam are incorporated in the attenuation constant, α. In addition, θ is the transmission phase shift of the DBR–free ring portion of half the MRR (the structure possesses symmetry in both x and y directions), K and S are the coupling and scattering matrices, respectively and defined as;

$$K = \begin{pmatrix} \tau & j\kappa \\ j\kappa & \tau \end{pmatrix} \tag{7}$$

$$S = \begin{pmatrix} S_{11} & S_{12} \\ S_{21} & S_{22} \end{pmatrix} = \begin{pmatrix} j|r|e^{j\phi} & |t| \\ |t| & j|r|e^{-j\phi} \end{pmatrix} e^{-j\psi} \tag{8}$$

where, κ and τ are coupling and transmission coefficients, respectively, of both waveguide–ring coupling points. Due to the lossless coupling condition we have that $\kappa^2 + \tau^2$=1. $|r|$ is the magnitude of the reflection coefficient and $|t|$ is the magnitude of the transmission coefficient of DBR set such that $|r|^2 + |t|^2$=1; ϕ is the reflection phase change and ψ is the transmission phase change of the DBRs. From equations (1)–(8) the outputs observed from Drop 1 (D_1) and Drop 2 (D_2) can be written, with the assumption of E_i=1, E_{-T}=0, D_{-1}=0 and D_{-2}=0 as,

$$D_1 = \frac{\kappa^2\tau^2\alpha^3 e^{j3\theta} S_{21} det(S) + \kappa^2 S_{12}\alpha e^{j\theta}}{\tau^2\alpha^2 e^{j2\theta}(S_{12}^2 + S_{21}^2 + 2S_{11}S_{22}) - (\tau^2\alpha^2 e^{j2\theta} det(S))^2 - 1} \tag{9}$$

$$D_2 = \frac{\kappa^2\tau\alpha^2 e^{j2\theta} S_{22}(S_{12} + S_{21})}{\tau^2\alpha^2 e^{j2\theta}(S_{12}^2 + S_{21}^2 + 2S_{11}S_{22}) - (\tau^2\alpha^2 e^{j2\theta} det(S))^2 - 1} \tag{10}$$

The total field phase change (Θ) for half a round trip (d_T) in the integrated micro–ring is determined by the transmission phase shift of the DBRs with length, d_{DBR} and the DBR–free micro-ring portion with length, d, as given by,

$$\Theta = \beta d_T = \beta(d_{DBR} + d) = \theta + \psi \tag{11}$$

where β is the propagation constant in the ring waveguide. The lengths of d_{DBR} and d are shown on a half MRR in Fig. 1(b) to make a clear definition of them. In this study, the DBRs occupy the entire micro–ring so there is no empty ring portion which leads to d=0, θ=0 and $d_T = d_{DBR}$. Thus, the total transmission phase shift after a half round trip is determined as,

$$\Theta = \beta d_{DBR} = \psi \tag{12}$$

The DBRs structure exhibits a reflection response under the assumption of a low reflectivity limit, neglecting multiple reflections, the reflection coefficient (spectral response of DBRs) is given by [20],

$$|r| = 2\xi N \frac{sin\Theta}{\Theta} \tag{13}$$

Here ξ is the reflection coefficient at each interface in a single discontinuity, so 2ξ per DBR period since there are two facets and N is the number of reflective elements in the DBR set. Thus, the counter propagating normalised mode intensities, $D_{1,2}$ of the ring-resonator have been calculated analytically by means of the theory presented above. They are shown in Fig. 2 with the assumption of α^2=0.8, ξ^2=1.15×10^{-4} (obtained by Fimmwave simulations for a single DBR period with the variables of D_{cy}=25% , w=500 nm and P=680 nm) and τ^2=0.99. The number of gratings is set to N=36 in order to satisfy the Bragg condition. Since the reflective elements are uniformly distributed throughout the MRR, the transmission and reflection phase change for half the ring is defined as Θ=πm and ϕ=πm where m is a random integer (for the purpose of resonance at the design wavelength) [16].

It is known that the DBRs produce a high reflectance at the design wavelength, which is known as the Bragg wavelength. In the light of this, it can be seen from Fig. 2

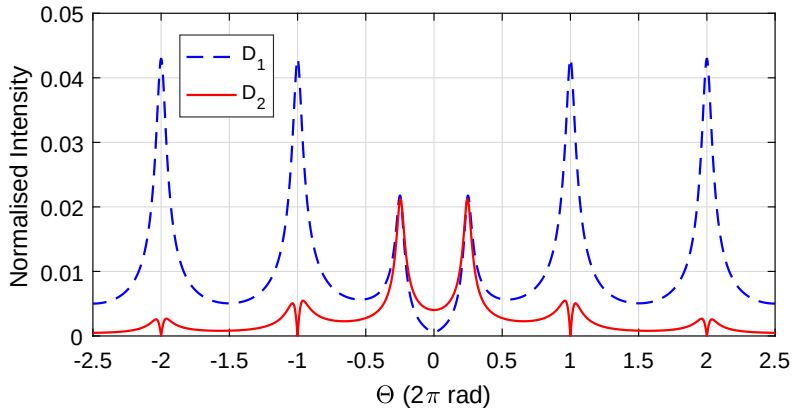

Figure 2: The output spectrum of D_1 and D_2 modes in case of ξ^2=1.15×10^{-4}.

that the intensity of the D_1 modes, the modes excited in the incident direction as shown in Fig. 1(a), are much higher than D_2 modes, the modes excited from reflected field in the MRR, for almost all displayed resonances except the one at the design wavelength where Θ=0. This means that the backscattering is comparable to the incident field at the design wavelength. Another noticeable feature observed in the spectrum is the splitting of the D_1 and D_2 resonant modes at the design wavelength. The main reason for this is the presence of the DBR on the MRR which causes the degeneracy between these two counter–propagating modes to be lifted [22]. This lifting of degeneracy results in symmetric doublets at the Bragg wavelength due to strong inter–resonance coupling of the D_1 and D_2 modes.

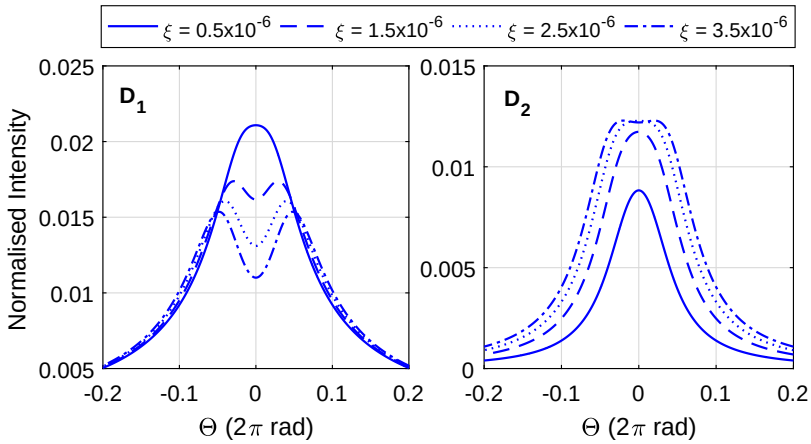

Figure 3: D_1 and D_2 outputs for different reflection ratios for the DBRs.

However, the splitting of each these modes are independent from each other in relation to reflection rate. Fig. 3 illustrates how 4 different levels of reflection can affect this doublet build up in the MRR. The figure shows that the backscattering plays a fundamental role in the split resonant mode structure. It is observed from

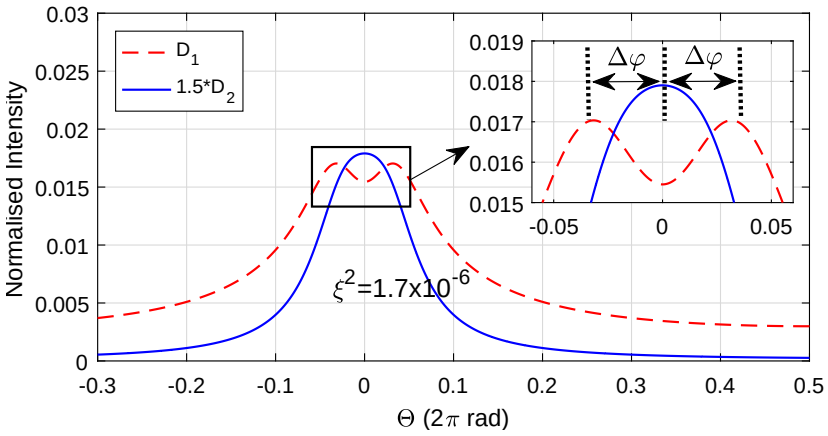

Figure 4: The spectra of D_1 and D_2 modes. Mode–splitting starts to take place for D_1 mode whereas the D_2 mode is still a single peak.

both Drop 1 and Drop 2 ports that a reflection coefficient of 0.5×10^{-6} produces a single resonant peak at the design wavelength. As this value reaches 1.5×10^{-6} the backscattering power becomes large enough to cause the D_1 modes to split, while for the D_2 modes a reflection coefficient of 3.5×10^{-6} is required. As observed in Fig. 4, when a reflection coefficient within the aforementioned window (1.5×10^{-6}–3.5×10^{-6}) occurs, a phase shift, $\Delta\varphi$ appears between the D_1 and D_2 modes at the design wavelength. As this coefficient increases from the lower to higher value, $\Delta\varphi$ increases and eventually mode splitting occurs for mode D_2 as well. In order to explain the operating principle in detail and validate the theoretical predictions, a 2D FDTD model is adopted and studied in following subsection.

2.2. Numerical Model

In this subsection, the analytically proposed model is investigated for an optical concentration sensor that monitor the concentration of a particular substance. In order to mimic the concentration of the substance in the cladding of MRR, nanometer–scale particles are utilised. The analytical model shown in Fig. 1(a) is created in a virtual platform utilising FDTD numerical modelling. The DBR–MRR model considered in the analytical calculation is a silicon device of ring radius R =4.0 μm with refractive index of n_1=3.477, based on the silicon-on-insulator (SOI) platform. The two access waveguides and the ring waveguide are all of 500 nm width. The construction of the DBR–MRR also includes 36 angular–gratings which are placed on the ring resonator and each element with w=500 nm , n_2=3.45 (n_2 is chosen in such a way that both D_1 and D_2 resonant modes are single peak) and D_{cy}=5%. The gratings are assumed to be the only part of DBR–MRR that attracts the analyte, this can be achieved using surface functionalisation. To simulate the attached particles in 2D calculations, small disks are placed in the grating region as shown Fig. 5.

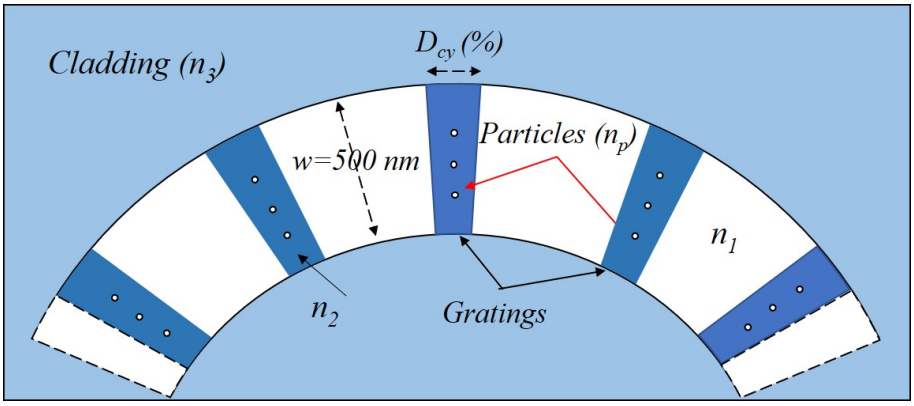

Figure 5: The figure shows a part of DBR–MRR image displaying the location of particles used in simulations. This shows the case for 36×3=108 particles uniformly distributed around the ring, P =680 nm and D_{cy}=5%, n_2= 3.45, n_1= 3.477, n_3= 1.318, n_P =1.5: Since the geometry is curved, the period (P) is defined as $2\pi R/N$.

MEEP software is used for the 2D FDTD simulations. The numerical calculations are performed with a fine grid size as small as 1 nm and sufficient operation time is used for high accuracy and reliability of the simulations. For the calculations, the DBR–MRR system is assumed to be placed in a water medium (n_3= 1.318 at Telecom wavelengths).

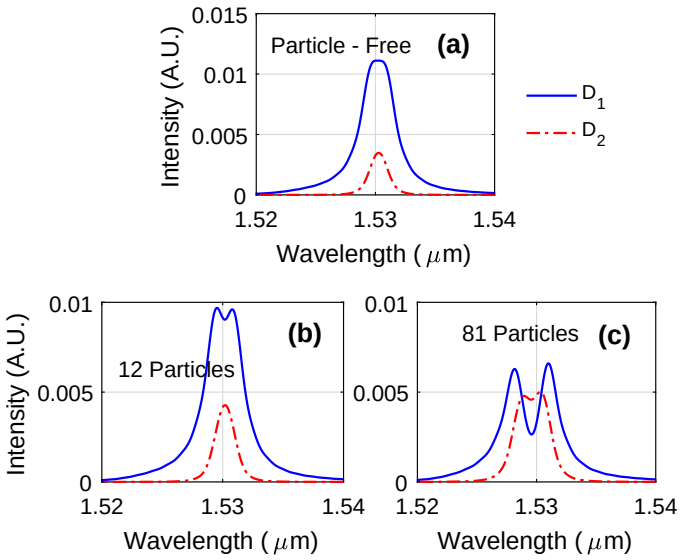

Figure 6: Spectral response of MRR in case of a-) 0%, b-) a% and c-) b% concentration levels which are simulated as an environment with no–particles, 12 particles and 81 particles both with 6nm radius bind to gratings, respectively

Fig. 6 illustrates the D_1 and D_2 resonant modes in case of three different particle concentrations placed uniformly around the ring. Fig. 6(a) shows the resonant modes of the MRR in a particle–free/zero concentration environment. It can be seen from

the figure that the resonant peaks of both D_1 and D_2 are single peaks. In addition, the magnitude of D_2 mode is around 1/4 of the D_1 mode. Fig. 6(b) shows that at a concentration level of $a\%$, which simulated as 12 particles with a random size of 6 nm radius and 1.5 refractive index attached uniformly to the ring, the single resonant peak of D_1 starts to split. However, mode–splitting starts to take place for D_2 at a concentration level of $b\%$ which simulated as 81 particles attached to the MRR as shown in Fig. 6(c).

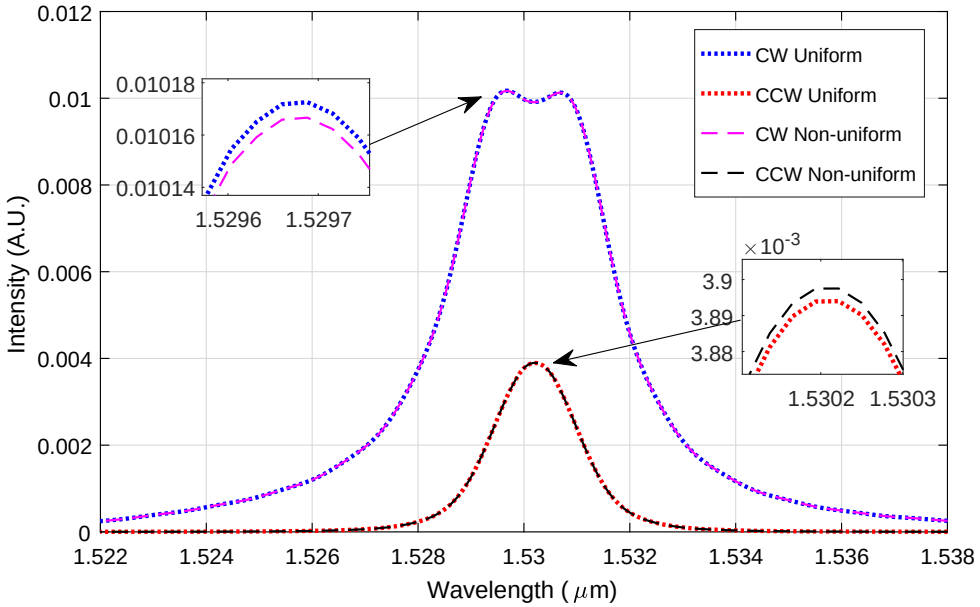

Figure 7: The role of uniform and non-uniform particle distributions on spectral response of the proposed geometry. 36 particles with 3nm radii for both uniform distribution: one particle placed on each grating, and, non-uniform distribution: No particles placed on first 6 gratings with two particles placed on each last 6 gratings and one particle for each remaining gratings. The magnified insets show no spectral shift but intensity change in CW and CCW modes.

From the Figs. 6(b–c) it is also clear that the magnitude of the D_2 modes increase as the concentration increases. This magnitude change and the splitting is due to the increment in backscattering power which is caused by the particle interference in the DBR–MRR [8, 23] and inter–modal coupling between D_1 and D_2 modes as explained analytically above.

In this study, it is assumed that the distribution of the particles around the device is uniform. The reason for a uniform distribution of particles here is to indicate a homogeneous mixture. Otherwise for a proper sensing operation the uniformity is not necessary since the distribution just effects the intensity change not the spectral change. The uniform and non–uniform distributions are demonstrated in Fig. 7 utilising 36 particles with 3nm radii attached to a device of 36 gratings. Such that, for the non–uniform distribution, the first 6 of the 36 gratings are left particle–free and the last 6 are

set to have two particles on each. The rest of the 36 particles placed with one particle on each grating. In case of the uniform distribution, however, one particle is placed on each of 36 gratings.

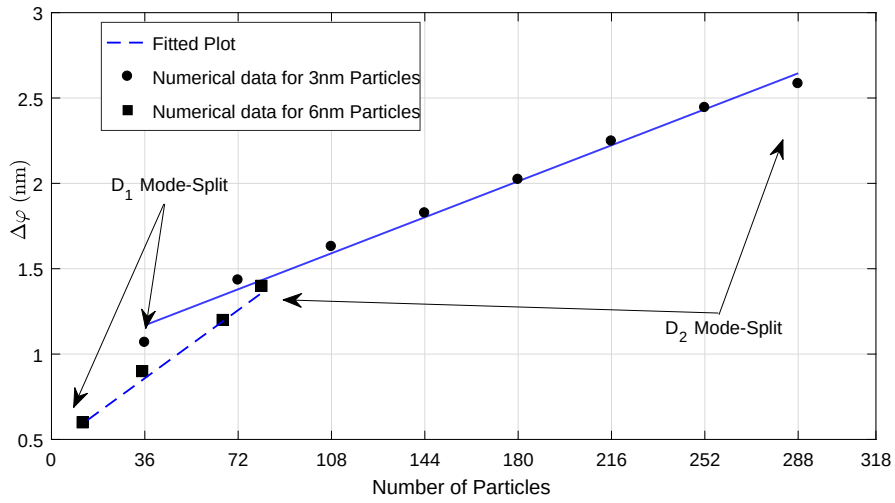

Figure 8: The evolution of $\Delta\varphi$ based on the number of bound particles with radius of 6 nm and 3 nm with a refractive index of 1.5.

Fig. 8 shows the mode–splitting evolution with regards to binding particles of 3 nm radius to the DBRs. It is observed that the smaller particles of a mixture scatter less power than relatively bigger ones, 6 nm in this case and cause the same resonant mode–splitting effect with relatively higher number of bindings. As seen from Fig. 8, binding of 36 particles to the DBRs (one particle to each grating) causes mode–splitting in D_1 and a $\Delta\varphi$ of $\approx$1.1 nm is observed. This value increases with a constant intake of particles, one particle attaches to each gratings at every sensing cycle, up to $\approx$2.6 nm until the split in D_2 mode starts to take place. After this point, both D_1 and D_2 modes will exhibit split–modes in their spectrum. One needs to note that $\Delta\varphi$ does not directly increase from zero when the mode–splitting commences. The theoretical analysis showed that $\Delta\varphi$ increased from a certain initial value during the splitting operation. Thus, in the case of a possible application, the exact initial values of $\Delta\varphi$ for the D_1 and D_2 modes needs to be identified for a proper operation mapping.

It is possible to tune the mode–splitting conditions simply by changing some characteristics of the device. Fig. 9 shows that the formation of the resonant mode is highly dependent on the refractive index, n_2, and D_{cy} of DBR gratings. It is difficult to select a value of n_2 to set the initial characteristics of both modes. However, regardless of the dimension of the geometry, this value can be adjusted with the aid of duty cycle as shown in Fig. 9. As seen from the Fig. 9, in case of the same concentration level, an environment of 12 particles, the DBRMRR device with n_2=3.46 and D_{cy}=5% forms a single peak of D_1 mode whereas an index of n_2=3.45 generates a mode–split with same

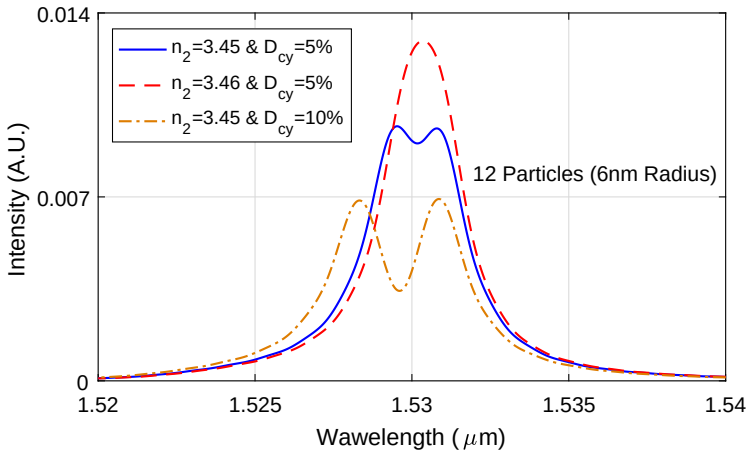

Figure 9: Splitting of resonant modes can be adjusted with the tuning of D_{cy} and/or refractive index of DBR gratings. The presented result is obtained from the simulations that performed employing the structures with n_1= 3.477 and three different n_2 in case of 12 particles with 6 nm radius.

D_{cy}. In addition, with a higher D_{cy} of 10% this split further increases. This means that the mode–splitting in the D_1 and D_2 modes can be adjusted in such a way that it occurs when the desired concentration levels of a% and b% are reached during the sensing operation. It also directly means that n_2 and duty–cycle are interrelated, and that each of both can be manipulated to tune one another.

3. Result and Discussion

It is understood from analytical and numerical outputs of the study that the backscattering power affects D_1 and D_2 modes at different levels to make their resonant modes split. The different degree of splitting of D_1 and D_2 modes which occurs at different reflection coefficient values can be utilised, in principle, to keep the concentration level of a particular substance within a desired range in a liquid environment. This can be done by associating the split of D_1 and D_2 modes to the lower (a%) and higher (b%) concentration levels of an analyte under investigation, respectively. The mode–splitting system can be adjusted in such a way that the split of D_1 mode occurs when the concentration level of a substance reaches to a%. The continuous rise in the concentration level, increases the $\Delta\varphi$ until the concentration reaches to b% where D_2 resonant mode–split takes place. Thus, one can visually monitor the concentration level of a particular substance by observing the spectra of the D_1 and D_2 modes. In addition, the Intermediate concentration values within desired range can be obtain by monitoring $\Delta\varphi$. It is observed from the numerical results that the mode–splitting happens in D_1 when a relatively small number of particles bind to the sensing layer of the sensor. For D_2, however, relatively higher number of particle is needed for the split to happen. This can be associated to the lower and higher level of desired concentration range,

respectively. With the indication of mode–splits in the spectrum, one can monitor the level of the concentration in a robust and easy way just to follow a screen. Adjustment to the parameters of n_2 and D_{cy} in the fabrication stage can be made to tune the splitting concentration levels for setting the desired range to control.

4. Conclusion

In summary, the spectrum of an DBR–MRR structure is studied analytically and numerically. Different splitting behaviours of D_1 and D_2 modes is demonstrated for the first time in literature and the concept applied to an optical sensor; concentration range sensor. Both numerical and analytical calculations suggest that the proposed structure could be a good candidate for concentration sensing which holds great potential for biological sensing applications on a SOI technology platform. In addition, not limited with the sensing application discussed here, there is no doubt that the presented new splitting concept of counter-propagating modes of MRR will lead future studies for a wide range of applications. Future work will carry out full 3D FDTD modelling in order to perform detailed device modelling and design prior to fabrication.

5. References

[1] Cicek K, Hu Z, Zhu J, Meriggi L, Li S, Nong Z, et al. Integrated optical vortex beam receivers. Optics Express. 2016;24:28529–28539.

[2] Makino T, i Gotoh T, Hasegawa R, Arakawa T, Kokubun Y. Microring resonator wavelength tunable filter using five-layer asymmetric coupled quantum well. Journal of Lightwave Technology. 2011;29:2387–2393.

[3] i Matsuo S, Segawa T. Microring-resonator-based widely tunable lasers. IEEE Journal of Selected Topics in Quantum Electronics. 2009;15:545–554.

[4] Wen YH, Kuzucu O, Hou T, Lipson M, Gaeta AL. All-optical switching of a single resonance in silicon ring resonators. Optics Letters. 2011;36:1413–1415.

[5] Cicek K, Eryrek M, Kiraz A. Single-slot hybrid microring resonator hydrogen sensor. Journal of the Optical Society of America B. 2017;34:1465–1470.

[6] Kim W, Ozdemir SK, Zhu J, Yang L. Observation and characterization of mode splitting in microsphere resonators in aquatic environment. Appl Phys Lett. 2011;p. 141106.

[7] Campanella CE, Giorgini A, Avino S, Malara P, Zullo R, Gagliardi G, et al. Localized strain sensing with fiber Bragg-grating ring cavities. Opt Express. 2013;21:29435–29441.

[8] Kim W, Ozdemir SK, Zhu J, He L, Yang L. Demonstration of mode splitting in an optical microcavity in aqueous environment. Appl Phys Lett. 2010;97:71111–71118.

[9] Zhu J, Ozdemir SK, He L, Chen DR, Yang L. Single virus and nanoparticle size spectrometry by whispering gallery mode microcavities. Optics Express. 2011;p. 16195–16206.

[10] Kim W, Ozdemir SK, Zhu J, Monifi F, Coban C, Yang L. Detection and size measurement of individual hemozoin nanocrystals in aquatic environment using a whispering gallery mode resonator. Opt Express. 2012;p. 2942629446.

[11] Zhu J, Ozdemir SK, Xiao Y, Lin L, He L, Chen D, et al. On-chip single nanoparticle detection and sizing by mode splitting in an ultrahigh-Q microresonator. Nature Photonics. 2009;4:46–49.

[12] Ozdemir SK, Zhu J, Yang X, Peng B, Yilmaz H, He L, et al. Highly sensitive detection of nanoparticles with a self-referenced and self-heterodyned whispering-gallery Raman microlaser. Proc Natl Acad Sci USA. 2014;p. E3836E3844.

[13] Malara P, Mastronardi L, Campanella CE, Giorgini A, Avino S, Passaro VMN, et al. Split-mode fiber Bragg grating sensor for high-resolution static strain measurements. Journal of Vibration and Acoustics. 2014;p. 6899–6902.

[14] Liu Y, Zhang L, Williams JAR, Bennion I. Optical Bend Sensor Based on Measurement of Resonance Mode Splitting of Long-Period Fiber Grating. IEEE Photonics Technology Letters. 2000;p. 531–533.

[15] Vallabhaneni AK, Rhoads JF, Murthy JY, Ruan X. Defect-Induced Mechanical Mode Splitting in Carbon Nanotube Resonators. Journal of Vibration and Acoustics. 2013;p. 024504–1.

[16] Kang YM, Arbabi A, Goddard LL. Engineering the spectral reflectance of microring resonators with integrated reflective elements. Opt Express. 2010;18:16813–16825.

[17] Leonardis F, Campanella CE, Troia B, Perri AG, Passaro VMN. Performance of SOI Bragg Grating Ring Resonator for Nonlinear Sensing Applications. Sensors. 2014;14:16017–16034.

[18] Gabalis M, Urbonas D, Petruskevicius R. A perforated microring resonator for optical sensing applications. Journal of Optics. 2014;p. 105003–6pp.

[19] Zhou L, Sun X, Li X, Chen J. Miniature microring resonator sensor based on a hybrid plasmonic waveguide. Sensors. 2011;p. 6856–6867.

[20] Coldren LA, Corzine SW, Mashanovitch ML. Diode Lasers and Photonic Integrated Circuits. Hoboken, NJ, USA: Wiley interscience; 2012.

[21] Kang YM, Goddard LL. A microring resonator with an integrated Bragg grating: a compact replacement for a sampled grating distributed Bragg reflector. Opt Quant Electron. 2009;p. 689–697.

[22] Li Q, Wang T, Su Y, Yan M, Qiu M. Coupled mode theory analysis of mode-splitting in coupled cavity system. Opt Express. 2010;p. 8367–8382.

[23] Weiss DS, Sandoghdar V, Hare J, Lefevre-Seguin V, Raimond JM, Haroche S. Splitting of high-Q Mie modes induced by light backscattering in silica microspheres. Optics Letters. 1995;p. 1835–1837.